Demosaicing enhancement using pixel-level fusion

CHIMAN KWAN

Journal of Signal, Image, and Video Processing

Signal, Image and Video Processing
https://doi.org/10.1007/s11760-017-1216-2

ORIGINAL PAPER

Demosaicing enhancement using pixel-level fusion

Chiman Kwan[1] · Bryan Chou[1] · Li-Yun M. Kwan[1] · Jude Larkin[1] · Bulent Ayhan[1] · James F. Bell III[2] · Hannah Kerner[2]

Received: 14 June 2017 / Revised: 22 September 2017 / Accepted: 22 November 2017

Abstract
Bayer pattern has been widely used in commercial digital cameras. In NASA's mast camera (Mastcams) onboard the Mars rover Curiosity, Bayer pattern has also been used in capturing the RGB bands. It is well known that debayering, also known as demosaicing in the literature, introduces artifacts such as false colors and zipper edges. In this paper, we first present four fusion approaches, including weighted and the well-known alpha-trimmed mean filtering approaches. Each fusion approach combines demosaicing results from seven debayering algorithms in the literature, which are selected based on their performance mentioned in other survey papers and the availability of open source codes. Second, we present debayering results using two benchmark image data sets: IMAX and Kodak. It was observed that none of the seven algorithms in the literature can yield the best performance in terms of peak signal-to-noise ratio (PSNR), CIELAB score, and subjective evaluation. Although the fusion algorithms are simple, it turns out that the debayering performance can be improved quite dramatically after fusion based on our extensive evaluations. In particular, the average PSNR improvements of the weighted fusion algorithm over the best individual method are 1.1 dB for the IMAX database and 1.8 dB for the Kodak database, respectively. Third, we applied the various algorithms to 36 actual Mastcam images. Subjective evaluation indicates that the fusion algorithms still work well, but not as good as the existing debayering algorithm used by NASA.

Keywords Debayering · Demosaicing · Fusion · Mastcam · Image enhancement

1 Introduction

The NASA Curiosity rover landed on Mars in 2012 after 8 months of journey [1]. The rover has several instruments onboard that can help characterize the Mars surface. The alpha particle X-ray spectrometer (APXS) [2] can analyze rock samples and extract compositions of rocks; the laser-induced breakdown spectroscopy (LIBS) [3,4] can collect spectral features from the vaporized fumes and deduce the rock compositions at a distance of 7 m; and Mastcam images [5–9] can perform surface characterization from 1 km away. There are two Mastcam multispectral images (9 bands in each images), separated by 24.2 cm [1]. Out of the 9 bands, the RGB bands are generated by using a Bayer pattern.

Bayer pattern was first invented in 1976 [10]. Over the years, many debayering algorithms have been developed. See two recent survey papers [11,12] and references therein. In a recent paper [13], an algorithm based on local directional interpolation and nonlocal search was developed. The performance was quite impressive for a benchmark data set known as IMAX [13]. In [13], the authors argued that many past algorithms used another benchmark data set called Kodak data set for evaluation where the Kodak images have good spectral correlations between bands. In many digital images, this is rarely the case, according to [13]. As a result, many algorithms that perform well for Kodak image set may not work well for the more challenging IMAX data. It will be important to find algorithms that can work well in both benchmark data sets.

For demosaicing the RGB bands, the current Mastcam uses Malvar–He–Cutler (MHC) algorithm [14], which was published in 2004, due to its simplicity. In Bell's paper [1], directional linear minimum mean square error estimation

Electronic supplementary material The online version of this article (https://doi.org/10.1007/s11760-017-1216-2) contains supplementary material, which is available to authorized users.

✉ Chiman Kwan
chiman.kwan@arllc.net

[1] Applied Research LLC, Rockville, MD, USA

[2] Arizona State University, Tempe, AZ, USA

Published online: 29 November 2017

Fig. 1 IMAX data set

Fig. 2 Kodak image set

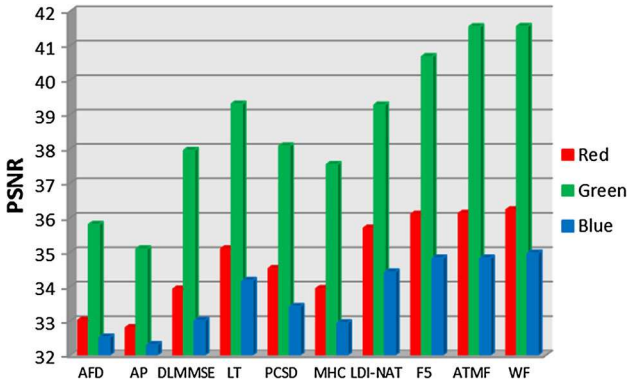

Fig. 3 Comparison of different algorithms using the IMAX images. Averaged PSNRs from all 18 images are used

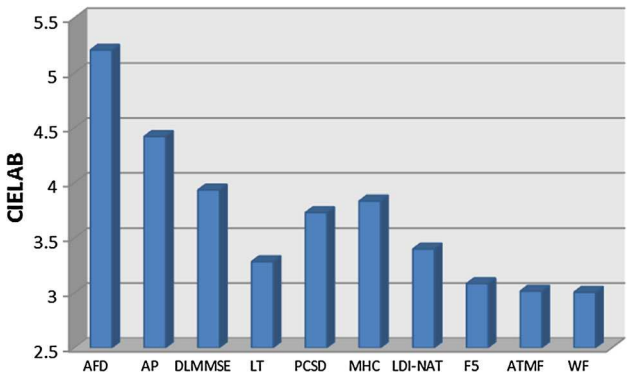

Fig. 4 Comparison of different algorithms using the IMAX images. Averaged CIELAB scores from all 18 images are used here

(DLMMSE) [15] was also evaluated. One motivation of our research was to explore whether or not there are better and effective algorithms since 2004 for demosaicing Mastcam images. Several algorithms [16–19] with publicly available codes were identified and compared. Another motivation was to investigate the performance of several fusion approaches. In Li et al.'s paper [11], a simple fusion approach with equal weights was applied and some notable improvement was observed. To the best of our knowledge, there is no systematic study on the use of pixe-level fusion for improving demosaiced images other than [11]. A systematic study of fusion methods is the first key contribution of our paper. In our study, we investigated four simple fusion approaches, including equal weighting, unequal weighting, random weighting, and a fusion scheme known as alpha-trimmed mean filtering (ATMF) that is widely used in sports and other applications [20]. Two benchmark image sets (IMAX and Kodak) were used in our studies. All of the demosaicing papers published in the last decade used either one of the two data sets for performance evaluations. It was found that among the seven algorithms, none of them works the best for both image sets. For the four fusion approaches, two of them outperformed the others. One good approach is ATMF [20] and the other good one is the weighted fusion. We also applied the various demosaicing algorithms to 36 Mastcam images, which were retrieved from the NASA Planetary Data System (PDS). It was observed that Malvar et al.'s algorithm [14] performed very well for Mastcam images even though it was not the best performing algorithm for both IMAX and Kodak images. The comparison of 10 debayering algorithms for the Mastcam images will be considered as the second major contribution of our research, as the observation is somewhat surprising. Without this systematic study, one may recommend other debayering algorithms to NASA for future Mastcam development.

This paper is organized as follows. In Sect. 2, we summarize the four fusion approaches. Section 3 summarizes the extensive experimental results, including the application of the various algorithms to the two benchmark data sets and 36 Mastcam images. Finally, concluding remarks and future research directions will be provided in Sect. 4.

Table 1 Summary of PSNR and CIELAB scores of various algorithms for all the IMAX images

Image	Criterion	AFD	AP	LT	DLMMSE	PCSD	MHC	LDI-NAT	FS	F5	WF
1	PSNR	25.916	25.647	28.855	27.465	28.076	27.759	29.256	29.931	**29.988**	29.975
	CIELAB	8.526	7.390	5.422	6.449	6.025	6.192	5.683	5.080	**4.981**	5.054
2	PSNR	32.941	32.708	35.134	34.276	34.603	33.748	35.302	36.422	36.356	**36.521**
	CIELAB	5.640	5.134	4.015	4.483	4.308	4.691	3.982	3.612	3.622	**3.593**
3	PSNR	32.346	31.689	33.514	32.860	32.573	31.526	33.325	35.243	33.489	**35.453**
	CIELAB	5.620	4.793	3.653	4.252	4.266	4.714	4.081	3.229	3.822	**3.202**
4	PSNR	35.137	33.203	37.001	34.586	34.821	33.910	36.709	38.271	36.242	**38.570**
	CIELAB	1.785	2.166	1.336	1.873	1.803	1.783	1.386	1.263	1.530	**1.262**
5	PSNR	30.051	29.899	33.425	31.635	32.389	32.247	33.951	34.213	**34.369**	34.233
	CIELAB	3.594	3.601	2.657	3.126	2.937	2.961	2.553	2.449	**2.420**	2.451
6	PSNR	32.762	32.294	37.168	34.913	35.937	35.844	37.649	37.869	**38.048**	37.664
	CIELAB	3.534	3.700	2.496	3.077	2.814	2.740	2.377	2.342	**2.301**	2.358
7	PSNR	38.335	37.914	37.182	38.761	37.141	35.315	36.849	40.163	39.954	**40.439**
	CIELAB	2.414	2.368	2.333	2.153	2.432	3.013	2.377	1.807	1.892	**1.778**
8	PSNR	37.023	36.823	37.808	37.955	38.099	36.480	38.110	40.121	38.454	**40.250**
	CIELAB	5.606	4.837	4.203	4.455	4.572	4.900	4.235	3.617	4.249	**3.599**
9	PSNR	33.992	33.673	36.768	35.259	35.908	35.783	37.473	37.967	38.004	**38.010**
	CIELAB	5.032	3.960	2.882	3.547	3.289	3.355	2.897	2.716	**2.679**	2.727
10	PSNR	35.350	34.960	37.941	36.752	37.377	37.167	38.488	39.385	39.373	**39.463**
	CIELAB	4.692	4.164	3.126	3.650	3.467	3.490	3.119	2.798	2.805	**2.789**
11	PSNR	36.436	36.053	39.066	37.702	38.195	38.272	39.491	40.370	40.331	**40.464**
	CIELAB	6.265	4.900	3.564	4.487	4.188	4.044	3.757	3.388	**3.352**	3.357
12	PSNR	35.939	35.807	38.328	36.930	37.397	36.509	38.536	39.667	39.549	**39.776**
	CIELAB	2.763	2.620	1.986	2.392	2.310	2.597	1.979	1.800	1.824	**1.799**
13	PSNR	37.692	37.533	40.858	39.330	39.722	39.233	41.201	41.842	**41.888**	41.864
	CIELAB	1.706	1.704	1.395	1.558	1.499	1.544	1.355	1.261	1.264	**1.250**
14	PSNR	36.462	36.558	38.826	37.885	38.151	37.690	38.984	39.902	39.878	**39.998**
	CIELAB	3.383	3.216	2.587	2.916	2.826	2.881	2.530	2.353	2.354	**2.333**
15	PSNR	36.657	36.540	38.764	37.777	38.146	38.026	39.139	40.000	39.981	**40.169**
	CIELAB	4.489	3.947	3.149	3.591	3.480	3.590	3.061	2.879	2.880	**2.878**
16	PSNR	29.350	29.230	33.293	31.075	31.992	31.928	33.396	33.965	**34.044**	33.930
	CIELAB	12.213	7.630	5.283	7.181	6.426	6.048	6.593	5.256	**5.146**	5.177
17	PSNR	28.621	27.971	31.859	29.798	30.938	31.509	32.783	32.912	**32.985**	32.891
	CIELAB	10.905	8.941	5.683	7.555	6.686	6.374	5.522	5.326	**5.294**	5.407
18	PSNR	33.116	32.756	35.626	34.424	34.679	33.585	35.709	36.792	36.727	**36.923**
	CIELAB	5.562	4.489	3.353	4.054	3.813	4.112	3.691	3.117	3.098	**3.094**
Average	PSNR	33.785	33.403	36.190	34.966	35.341	34.807	36.464	37.502	37.203	**37.589**
	CIELAB	5.207	4.420	3.285	3.933	3.730	3.835	3.399	3.016	3.084	**3.006**

Bold values indicate the best performing algorithm for each row

2 Fusion approaches

Here, we briefly describe four fusion approaches, which are simple and intuitive. Although the ideas are simple, it turns out that the performance improvement is quite significant, as will be seen in Sect. 3. Simple and effective methods are invaluable in engineering applications, and proposing such simple solutions is one of our key contributions.

2.1 Fusion using equal weights

Suppose there are N demosaiced images generated by N different algorithms. This fusion approach works as follows.

At each pixel location (i, j), compute the mean of pixels at that location from all the N demosaiced images. Mathematically, this is expressed as

$$\bar{M}(i,j) = \frac{\sum_{n=1}^{N} M_n(i,j)}{N}, \tag{1}$$

where $M_n(i, j)$ is the pixel magnitude at (i, j) location of the nth demosaiced image. The resulting image is the fused image.

This approach was used in [11], and some noticeable improvement has been observed.

2.2 Fusion using random weights

In (1), all weights are the same and equal to $1/N$. Since the optimal set of weights is not known a priori, a weight search can be performed to determine the optimal weights. N random number generators can be used. Each one generates a number between [0, 1]. The random weights are then normalized to 1. That is, the fused pixels at location (i, j) are generated by using

$$\bar{M}(i, j) = \frac{\sum_{n=1}^{N} w_n M_n(i, j)}{N}, \tag{2}$$

where $\sum w_n = 1$. This algorithm requires some training data. Given some representative images, one can perform many experiments. Based on the results, the best set of weights can be selected. However, the search time can be very lengthy.

2.3 Fusion using weighted average

Similar to the random weight approach, weighted average fusion also requires some training images. The mean squared errors (MSE) or peak signal-to-noise ratio (PSNR) or some other performance metrics are generated for all debayering algorithms. Based on the performance metrics, one can derive a set of weights. For example, if one uses MSE, then one potential weight selection strategy is as follows:

$$w_n = 1/\mathrm{MSE}(n), \quad n = 1, \ldots, N. \tag{3}$$

The weights are then normalized to 1. Equation (2) can then be used to generate the fused image. In our studies, we found that using MSE yielded better performance than other metrics.

2.4 Fusion using alpha-trimmed mean filtering [20]

The alpha-trimmed mean approach described in [20] is based on order statistics and has been widely used in sports and other applications. Out of N scores from judges, the highest and lowest scores are deleted and the mean of the remaining scores will be used as the final score. We adapt the above scheme to this application.

The steps are as follows:

Step 1 At each pixel location (i, j), the pixels from N demosaiced images are ranked based on magnitude.

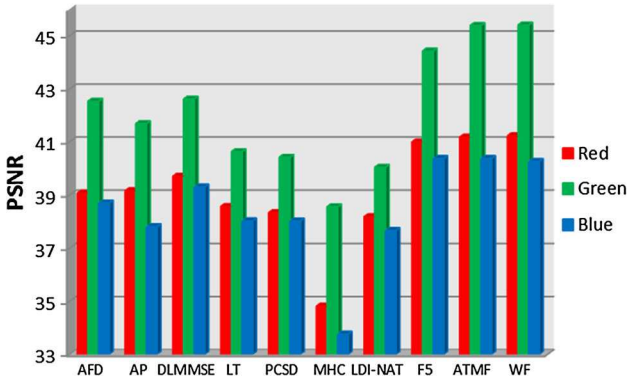

Fig. 5 Comparison of different algorithms using the Kodak images. Averaged PSNRs from all 12 images are used

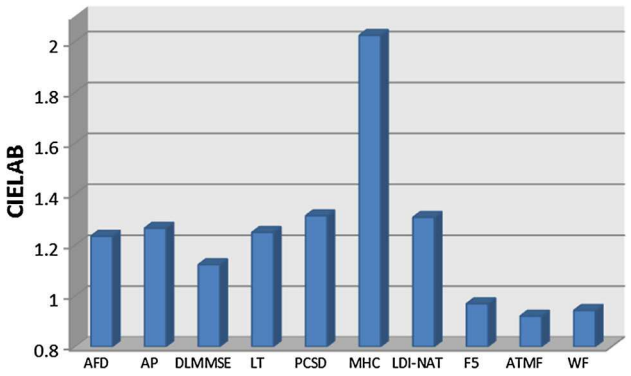

Fig. 6 Comparison of different algorithms using the Kodak images. Averaged CIELAB scores from all 12 images are used here

Step 2 The largest and smallest pixels are removed.

Step 3 The mean of the remaining pixels is then used as the fused value at (i, j).

This approach does not require any training images and it turns out that this is one of the best approaches in our extensive evaluations.

3 Experimental results

3.1 Data

We used two image data sets: IMAX and Kodak. Both are well known in debayering research community. There are 18 images in IMAX (Fig. 1) and 12 images in Kodak (Fig. 2). In addition, we also used 36 actual Mastcam images to compare different debayering algorithms.

3.2 Performance metrics and demosaicing algorithms

Two performance metrics were used: peak signal-to-noise ratio (PSNR) and CIELAB [21]. It should be noted that

Table 2 Summary of PSNR and CIELAB scores of various algorithms for Kodak images

Image	Criterion	AFD	AP	LT	DLMMSE	PCSD	MHC	LDI-NAT	FS	F5	WF
1	PSNR	42.354	42.009	42.902	43.534	42.590	41.159	43.049	45.796	43.955	**45.823**
	CIELAB	0.947	0.981	0.905	0.874	0.962	1.092	0.893	**0.701**	0.836	0.703
2	PSNR	40.335	38.770	37.162	40.344	38.010	33.647	36.365	41.133	**41.285**	41.036
	CIELAB	1.128	1.253	1.327	1.047	1.297	2.289	1.421	0.951	**0.946**	0.981
3	PSNR	42.434	41.940	42.799	42.672	41.601	39.662	42.721	45.358	44.973	**45.401**
	CIELAB	1.129	1.136	0.989	1.019	1.120	1.437	1.011	**0.783**	0.825	0.794
4	PSNR	35.571	35.531	34.452	36.237	34.410	29.610	33.566	**38.030**	37.728	37.970
	CIELAB	1.821	1.847	1.863	1.600	1.928	3.646	2.001	**1.322**	1.384	1.376
5	PSNR	42.174	41.867	41.865	43.202	41.950	38.287	41.625	45.283	44.882	**45.285**
	CIELAB	0.885	0.851	0.834	0.741	0.816	1.238	0.853	**0.585**	0.619	0.592
6	PSNR	39.943	39.264	38.527	40.143	38.260	34.953	37.929	41.822	41.626	**41.889**
	CIELAB	1.492	1.490	1.474	1.305	1.600	2.547	1.572	**1.082**	1.133	1.110
7	PSNR	43.996	42.007	40.379	43.875	41.565	36.800	39.557	44.558	**44.792**	44.371
	CIELAB	0.883	1.044	1.110	0.852	1.059	1.825	1.192	0.790	**0.784**	0.817
8	PSNR	40.527	39.994	39.428	41.150	39.362	34.065	38.852	**42.980**	42.681	42.905
	CIELAB	1.236	1.289	1.287	1.114	1.332	2.251	1.361	**0.911**	0.951	0.929
9	PSNR	40.768	41.124	40.935	41.615	40.083	37.581	40.630	43.573	43.220	**43.639**
	CIELAB	1.113	1.013	0.985	0.945	1.096	1.528	1.030	**0.706**	0.805	0.778
10	PSNR	39.026	39.146	37.785	39.267	37.175	34.464	37.238	40.842	40.654	**40.903**
	CIELAB	1.344	1.323	1.393	1.251	1.528	2.266	1.459	**1.039**	1.070	1.050
11	PSNR	38.235	37.881	38.264	38.546	37.592	35.610	37.942	40.700	40.333	**40.875**
	CIELAB	1.414	1.520	1.416	1.397	1.519	1.967	1.450	1.097	1.152	**1.091**
12	PSNR	35.868	35.133	34.473	35.900	34.561	32.753	34.128	37.391	37.045	**37.516**
	CIELAB	1.430	1.455	1.416	1.330	1.526	2.204	1.465	**1.079**	1.129	1.093
Average	PSNR	40.103	39.556	39.081	40.540	38.930	35.716	38.634	42.289	41.931	**42.301**
	CIELAB	1.235	1.267	1.250	1.123	1.315	2.024	1.309	**0.921**	0.969	0.943

Bold values indicate the best performing algorithm for each row

these metrics have been widely used in many debayering papers.

Ten algorithms were used here. We list the algorithms below:

- Linear directional interpolation and nonlocal adaptive thresholding (LDI-NAT): It is the method from [13].
- MHC: It is the Malvar–He–Cutler algorithm in [14].
- Directional linear minimum mean square error estimation (DLMMSE): It is the Zhang and Wu algorithm in [15].
- Lu and Tan interpolation (LT): It is the algorithm from [16].
- Adaptive frequency domain (AFD): It is the algorithm from Dobois [17].
- Alternate projection (AP): It is the algorithm from Gunturk et al. [18].
- Primary-consistent soft-decision PCSD: It is the Wu and Zhang's algorithm [19].
- Alpha-trimmed mean filtering (ATMF): This method came from [20]. At each pixel location, we have pixels from seven methods; the largest and smallest pixels are removed, and the mean of the remaining pixels are used. This method fuses the results from AFD, AP, LT, DLMMSE, MHC, PCSD, and LDI-NAT.
- Fusion using 5 best (F5): Here, for IMAX, the mean of LT, DLMMSE, MHC, LDI-NAT, PCSD was used; for Kodak, the mean of AFD, AP, DLMMSE, LT, and PCSD was used.
- Weighted fusion (WF): Based on a training image, the MSEs of the seven algorithms (LT, AP, AFD, DLMMSE, LT, MHC, and LDI-NAT) are computed. The weights of each method are set to 1/MSE(i), where i is the index of the method. Those weights are then normalized to one. After that, the normalized weights are used at each pixel location to generate a weighted average image.

We did not include fusion results from random weighting, as the performance is not as good as the other fusion methods. Most importantly, the weight search takes many hours to finish.

3.3 Comparison of different algorithms using the IMAX images

Figure 3 summarizes the averaged PSNRs of all the 18 images from the ten demosaicing algorithms. The RGB bands are separated. Figure 4 summarizes the averaged CIELAB scores from the 18 images. Table 1 summarizes the PSNR and CIELAB results for all of the 18 images using the ten algorithms. From Figs. 3, 4, and Table 1, we have the following observations:

- Without fusion, LDI-NAT performed the best, followed by LT.
- With fusion, the method using WF yielded the best performance, followed by F5. Only image 1 was used for training for the WF approach.
- The averaged improvement in the WF method over the best individual method (LDI-NAT) is 1.1 dB, which is quite significant.

Figure 1 in the Supplement shows the demosaiced images using different algorithms for one of the images in the data set. The last one is the original. It can be seen that the images based on fusion have minimal artifacts as compared to each individual algorithm.

3.4 Comparison of different algorithms using the Kodak images

The Kodak images have more correlation between bands and hence are easier to demosaic as compared to that of IMAX images. Figure 5 summarizes the averaged PSNRs of those 12 Kodak images using ten algorithms. Figure 6 summarizes the CIELAB scores of the 12 images using 10 algorithms. Table 2 summarizes detailed PSNR and CIELAB scores for each image. From Figs. 5, 6, and Table 2, it can be seen that:

- Without fusion, AFD and DLMMSE have the best performance in terms of PSNR. However, DLMMSE has better performance than AFD in terms of CIELAB score.
- With fusion, ATMF method and weighted fusion results are slightly better in terms of PSNR. In terms of CIELAB, ATMF is slightly better. However, weighted fusion requires training. In our experiments, only the first image was used for getting the weights.
- The averaged improvement in the weighted fusion over the best individual method (DLMMSE) is 1.8 dB in terms of PSNR, which is also impressive.

Figure 7 shows the demosaiced images using the famous Lighthouse image. It can be seen that images using fusion methods have no observable artifacts.

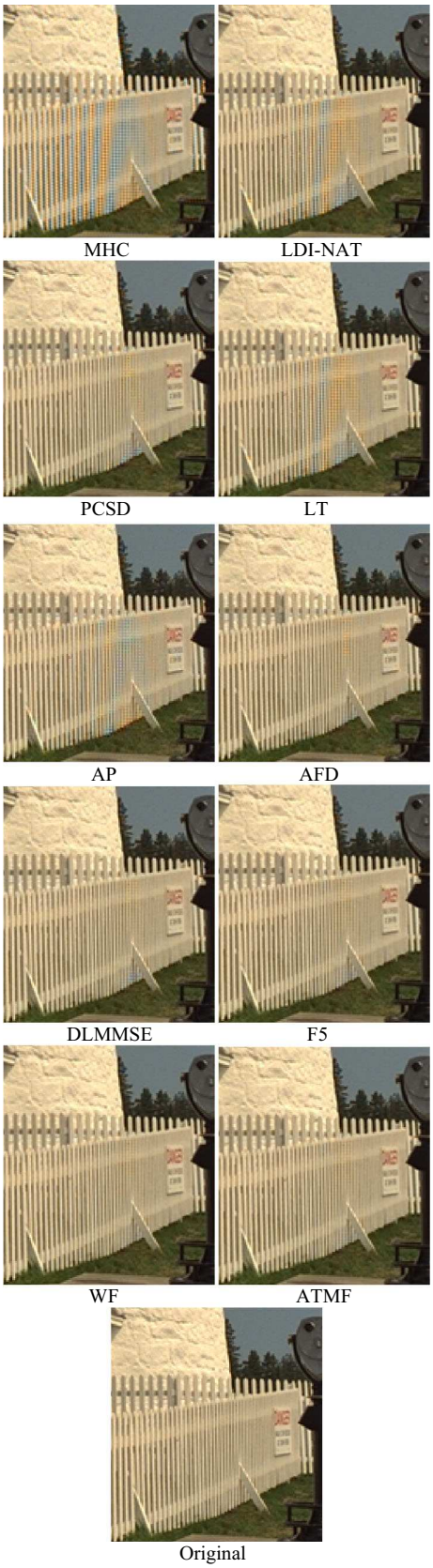

Fig. 7 Visual comparison of demosaiced images of different demosaicing algorithms

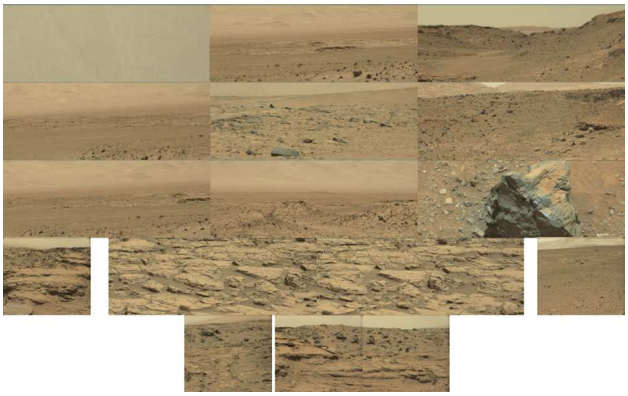

Fig. 8 Images from the left Mastcam

Fig. 9 Images from the right Mastcam

3.5 Application of demosaicing algorithms to actual Mastcam images

From the NASA's Planetary Data System (PDS), we have retrieved 31 actual Mastcam images, which were losslessly compressed and saved in Bayer pattern. Figures 8 and 9 show 16 left Mastcam images and 15 right Mastcam images, respectively. All of the debayered images using various algorithms have been subjectively evaluated. Since there are no ground truth images, we cannot generate PSNR and CIELAB metrics. Due to page limitation, we only include two exemplar demosaiced images below for subjective evaluation. Figures 10 and 11 show the debayered images using different algorithms for a left Mastcam image and a right Mastcam image, respectively. The F3 method fuses the results from LT, LDI-NAT, and MHC. Weighted fusion (WF) was not applied because no MSE can be generated without ground truth images. Figures 2 and 3 in the Supplement are two addi-

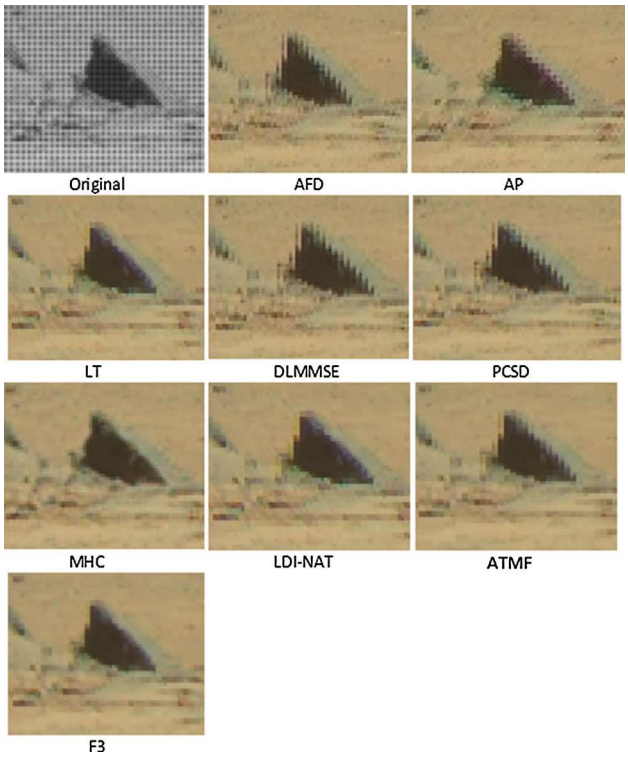

Fig. 10 Visual comparison of demosaiced images of different algorithms for a left Mastcam image

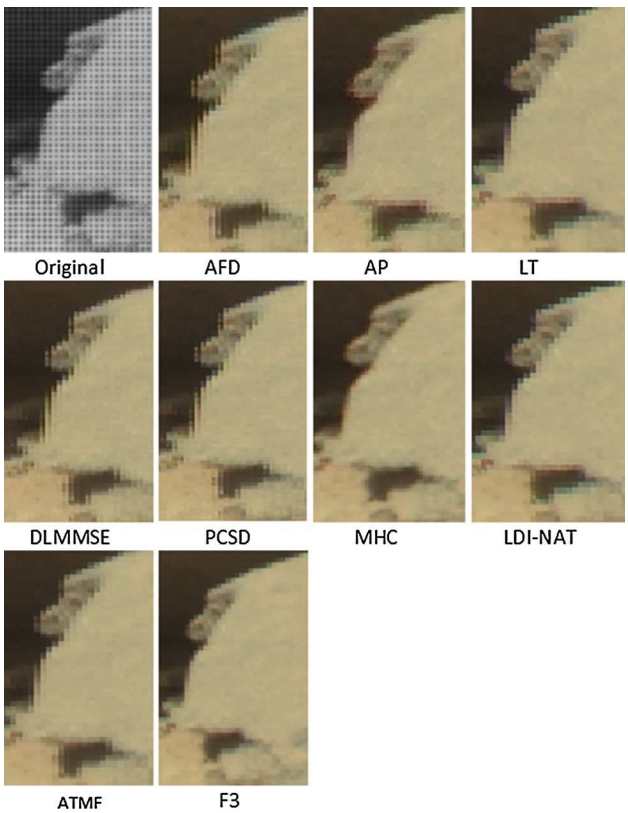

Fig. 11 Visual comparison of demosaiced images of different algorithms for a right Mastcam image

tional examples of debayering using Mastcam images. It can be seen that although the MHC algorithm was developed in 2004, it still performed quite well for all the Mastcam images. This is a surprise in our research, as MHC is so simple and yet its performance is so good for this NASA application. This is probably why NASA selected it in the first place. The surprising part is also because MHC does not perform that well in both the IMAX and Kodak images.

4 Conclusion

In this paper, we first present four simple fusion approaches to improve demosaicing performance. Each approach fuses some state-of-the-art debayering algorithms in the literature. Extensive experiments using two benchmark image sets were used for evaluations. It was observed that none of the individual algorithms can consistently work well for all images. The weighted fusion approach based on weighted fusion consistently worked well. However, one image is needed to get the weights. Another fusion approach based on alpha-trimmed mean filtering also performed very well. No training is required for this latter approach.

Based on our investigations for the actual Mastcam images, it is concluded that the Malvar–He–Cutler algorithm developed in 2004 performed the best for the Mastcam application despite the emergence of many new algorithms in recent years. The individual demosaicing algorithms without fusion that performed well for IMAX and Kodak images do not work that well for Mastcam images. One lesson learned from this study is that every application is unique, and it is necessary to investigate and compare different algorithms in order to select the most appropriate algorithm for a given application.

One potential future direction is to apply the fusion algorithms to CFA2.0 [22].

Acknowledgements This research was supported by NASA under Contract No. NNX16CP38P. Any opinions, findings, and conclusions or recommendations expressed in this material are those of the author(s) and do not necessarily reflect the views of NASA.

References

1. Bell III, J.F., et al.: The Mars Science Laboratory Curiosity Rover Mast Camera (Mastcam) Instruments: pre-flight and in-flight calibration, validation, and data archiving. AGU J. Earth Space Sci. **4**(7), 396–452 (2017)
2. Ayhan, B., Kwan, C., Vance, S.: On the use of a linear spectral unmixing technique for concentration estimation of APXS spectrum. J. Multidiscipl. Eng. Sci. Technol. **2**(9), 2469–2474 (2015)
3. Wang, W., Li, S., Qi, H., Ayhan, B., Kwan, C., Vance, S.: Revisiting the preprocessing procedures for elemental concentration estimation based on CHEMCAM LIBS on MARS Rover. In: 6th Workshop on Hyperspectral Image and Signal Processing: Evolution in Remote Sensing. (WHISPERS), Lausanne, Switzerland (2014)
4. Wang, W., Ayhan, B., Kwan, C., Qi, H., Vance, S.: A novel and effective multivariate method for compositional analysis using laser induced breakdown spectroscopy. In: 35th International Symposium on Remote Sensing of Environment (2014)
5. Dao, M., Kwan, C., Ayhan, B., Bell III, J.F.: Enhancing Mastcam images for Mars Rover mission. In: 14th International Symposium on Neural Networks, Hokkaido (2017)
6. Ayhan, B., Dao, M., Kwan, C., Chen, H., Bell, J., Kidd, R.: A novel utilization of image registration techniques to process Mastcam images in Mars Rover with applications to image fusion, pixel clustering, and anomaly detection. IEEE J. Select. Top. Appl. Earth Observ. Remote Sens. **10**(10), 4553–4564 (2017)
7. Kwan, C., Budavari, B., Dao, M., Ayhan, B., Bell, J.: Pansharpening of Mastcam images. In: IEEE International Geoscience and Remote Sensing Symposium, Fort Worth (2017)
8. Kwan, C., Dao, M., Chou, B., Kwan, L.M., Ayhan, B.: Mastcam image enhancement using estimated point spread functions. In: IEEE Ubiquitous Computing, Electronics and Mobile Communication Conference, New York City (2017)
9. Qu, Y., Guo, R., Wang, W., Qi, H., Ayhan, B., Kwan, C., Vance, S.: Anomaly detection in hyperspectral images through spectral unmixing and low rank decomposition. In: IEEE International Geoscience and Remote Sensing Symposium. IGARSS), Beijing (2016)
10. Bayer, B.: Color imaging array, US Patent 3,971,065 (1976)
11. Li, X., Gunturk, B., Zhang, L.: Image demosaicing: a systematic survey. In: Proceedings of SPIE, vol. 6822, Visual Communications and Image Processing (2008)
12. Lesson, O., Macaire, L., Yang, Y.: Comparison of color demosaicing methods. In: Hawkes, Peter W. (ed.) Advances in Imaging and Electron Physics, vol. 162, pp. 173–265. Elsevier, Amsterdam (2010)
13. Zhang, L., Wu, X., Buades, A., Li, X.: Color demosaicking by local directional interpolation and nonlocal adaptive thresholding. J. Electron. Imaging **20**(2), 023016 (2011)
14. Malvar, H., He, L.-W., Culter, R.: High-quality linear interpolation for demosaicking of color images. In: Proceedings of IEEE International Conference of Acoustics, Speech and Signal Processing, pp. 485–488 (2004)
15. Zhang, L., Wu, X.: Color demosaicking via directional linear minimum mean square-error estimation. IEEE Trans. Image Process. **14**(12), 2167–2178 (2005)
16. Lu, W., Tan, Y.: Color filter array demosaicking: new method and performance measures. IEEE Trans. Image Process. **12**(10), 1194–1210 (2003)
17. Dubois, E.: Frequency-domain methods for demosaicking of Bayer-sampled color images. IEEE Signal Proc. Lett. **12**(12), 847–850 (2005)
18. Gunturk, B., Altunbasak, Y., Mersereau, R.: Color plane interpolation using alternating projections. IEEE Trans. Image Process. **11**(9), 997–1013 (2002)
19. Wu, X., Zhang, N.: Primary-consistent soft-decision color demosaicking for digital cameras. IEEE Trans. IP **13**(9), 1263–1274 (2004)
20. Bednar, J., Watt, T.: Alpha-trimmed means and their relationship to median filters. IEEE Trans. Acoust. Speech Signal Process. **32**(1), 145–153 (1984)
21. Zhang, X., Wandell, B.: A spatial extension of CIELAB for digital color image reproduction. SID J. **5**(1), 61–63 (1997)
22. Kwan, C., Chou, B., Kwan, L. M., Budavari, B.: Debayering RGBW color filter arrays: a pansharpening approach. In: IEEE Ubiquitous Computing, Electronics and Mobile Communication Conference, New York City (2017)